


# Estimating various losses in c-Si solar cells subjected to partial shading: insights into $J$ – $V$ performance reduction

Zeel Purohit<sup>1</sup> · Harsh Chaliyawala<sup>2</sup> · Manoj Kumar<sup>1</sup> · Brijesh Tripathi<sup>1</sup> 

© Springer Science+Business Media, LLC, part of Springer Nature 2018

## Abstract

This article reports the effect of partial shading (PS) on the electrical output of a solar cell using the two-diode model. The reduction in electrical performance parameters induced by various recombination losses has been explained for c-Si solar cells under the effect of PS. The PS mainly affects the short-circuit current density ( $J_{SC}$ ) and efficiency ( $\eta$ ) of the solar cells.  $J_{SC}$  and  $\eta$  decrease from 37.84 to 5.48 mA cm<sup>-2</sup> and from 18.31 to 2%, respectively. Among all the energy losses encountered for PS, spatial relaxation and recombination losses are the dominating factors responsible for the reduction in  $J_{SC}$ . PC1D and Griddler simulations have been performed to evaluate the effect of front surface and bulk recombination. The PC1D simulated external quantum efficiency is governed by the front and back surface recombination velocity and carrier life time of the charge carriers under PS. The power loss ( $P_e$ ) of  $\sim 34\%$  from the emitter region has been determined by resistance analysis in correlation with the recombination in the emitter region of the solar cells under PS.

**Keywords** Solar photovoltaic · Partial shading (PS) · Two-diode model · External quantum efficiency (EQE) · PC1D and Griddler simulation

## 1 Introduction

Research and development studies of photovoltaic (PV) systems are mainly focused on the solar resource assessment, efficient operating strategies and their design and sizing. The electrical performance of a PV system is strongly affected by the climatic conditions such as changes in humidity, temperature, pollution and dust particle accumulation as reported in the last few years [1–7]. There are various other factors such as bird dropping, leaves and dust patches which create local shadowing effect and thus reduce the solar cell electrical output due to the variations in solar spectral intensity distribution [8–12]. Elminir et al. [13] reported the effect of dust

particles on the overall Si solar cell performance wherein, the panels have been installed at 45° angle facing the south and undergo the reduction of power output  $\sim 17.4\%$  per month due to accumulation of dust on their surface. Ghazi et al. [14] investigated the pattern of dust distribution in different parts of the world and found that the Middle East and North Africa have the worst dust accumulation zones in the world.

According to the recent studies, the partial shading (PS) on the surface of the PV panel affects the overall energy output from the PV power plant on a daily, monthly, seasonal and annual basis [15–19]. The power loss of a solar PV panel/cells can vary from 10 to 70% due to PS [20]. There are various reports on the electrical performance of Si solar cells and panels under PS conditions [21–26]. Vijayalekshmy et al. proposed a novel zigzag scheme for power enhancement of partially shaded solar arrays [26]. Liu et al. presented an overview of maximum power point tracking methods of PV power system for PS [27]. Quaschingt and Hanitscht have presented a numerical simulation of current density–voltage ( $J$ – $V$ ) characteristics of PV system with the shaded solar cells [28]. Ji et al. [29] have developed a real maximum power point tracking method for mismatching compensation in photovoltaic array under PS. Alajmi et al. [30] outlined a maximum power point tracking technique

**Electronic supplementary material** The online version of this article (<https://doi.org/10.1007/s10825-018-1158-0>) contains supplementary material, which is available to authorized users.

✉ Brijesh Tripathi  
brijesh.tripathi@sse.pdpu.ac.in

<sup>1</sup> Department of Science, School of Technology, Pandit Deendayal Petroleum University, Gandhinagar 382007, India

<sup>2</sup> Solar Research and Development Centre, School of Technology, Pandit Deendayal Petroleum University, Gandhinagar 382007, India

for partially shaded PV systems in micro-grids. To avoid and mitigate the consequence of shading such as hot spot, a bypass diode provision has been made in solar panels [31]. In addition to these, there are various reports which give an overview of the major impact of PS on the module level performance [32–38]. However, the fundamental concept behind the losses associated to the PS at single PV cell level has not been very well explored till now.

This paper presents both the experimental and theoretical aspects of the reduction in  $J$ – $V$  performance of c-Si solar cell subjected to PS. The significant deviation in  $J$ – $V$  performance has been evaluated by employing two-diode model, PC1D and Griddler simulation software. In addition, the energy balance losses are calculated to provide direct evidence of recombination associated to PS. The PC1D simulation has been carried out to further investigate the reduction in  $J_{SC}$  under PS. Further, external quantum efficiency (EQE) influenced by the front and back surface recombination has been correlated to the reduction in  $J$ – $V$  performance of solar cells under PS. In order to explore the losses associated to the front emitter region, the resistance analysis has been performed.

## 2 Theoretical considerations

The solar cell under full illumination (FI) ( $1000 \text{ W m}^{-2}$ , AM1.5G spectrum) shows nonlinear current–voltage ( $J$ – $V$ ) characteristics in a pseudo-rectangular shape. A deviation from this shape under PS leads to significant decrease in the maximum power output. The decreased nonlinearity is mainly due to the loss of photo-generated charge carriers. Various possible loss mechanisms of photo-generated charge carriers have been proposed by many researchers [39–43]. Among all the possible recombination losses, the radiative loss mechanism involves radiative recombination of electron–hole (e–h) pairs, and non-radiative recombination

mechanism involves the Shockley–Read–Hall, Auger and surface recombination [44]. The loss of photo-generated carriers can be estimated by using two-diode model as shown in Fig. 1, where the rectifying behavior of the P–N junction due to quasi-neutral region (QNR) and charge carrier recombination losses in space charge region (SCR) of a solar cell are represented by diode 1 and diode 2, respectively [45].

The nonlinear  $J$ – $V$  characteristics of the solar cell can be estimated with following terminal equation:

$$J_{FI} = J_{ph} - J_{D1} - J_{D2} - \frac{(V + JR_s)}{R_{sh}} \quad (1)$$

$$J_{D1} = J_i \left\{ \exp \left( \frac{q(V + JR_s)}{nk_B T} \right) - 1 \right\} \quad (2)$$

$$J_{D2} = J_r \left\{ \exp \left( \frac{q(V + JR_s)}{mk_B T} \right) - 1 \right\} \quad (3)$$

where  $J_{D1}$  and  $J_{D2}$  represent the current density of diode 1 and 2,  $n$  and  $m$  signifies the corresponding ideality factors.  $J_i$  and  $J_r$  indicates the dark saturation current density of the rectifying and recombination diodes, respectively [45],  $k_B$  represents the Boltzmann's constant,  $T$  represents the absolute temperature of the solar cell,  $q$  represents the electron charge,  $R_s$  represents the series resistance, and  $R_{sh}$  represents the shunt resistance.

In order to estimate the series resistance and power loss in the emitter region of a solar cell under PS, following expression has been used, assuming a combination of resistances shown schematically in Fig. 2 [46,47]:

$$R_s = R_{bus} + R_{bulk} + R_{pp+} + R_{Al} + \frac{R_c}{1 + \left( \frac{R_c}{R_p} \right)} \quad (4)$$

where  $R_{bus}$  represents busbar resistance,  $R_{bulk}$  indicates bulk region resistance,  $R_{pp+}$  represents the silicon bulk and Al back electrode interface,  $R_{Al}$  represents back electrode,  $R_c$

Fig. 1 Two-diode model circuit

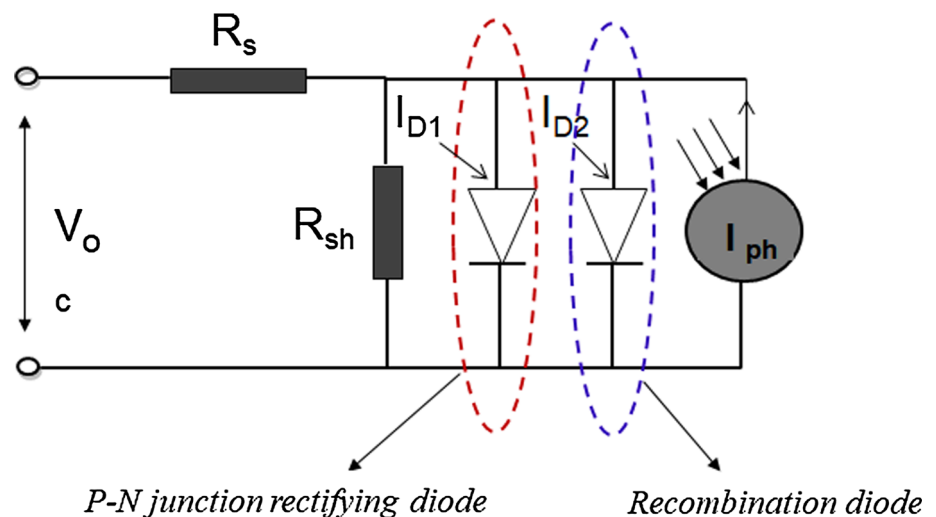
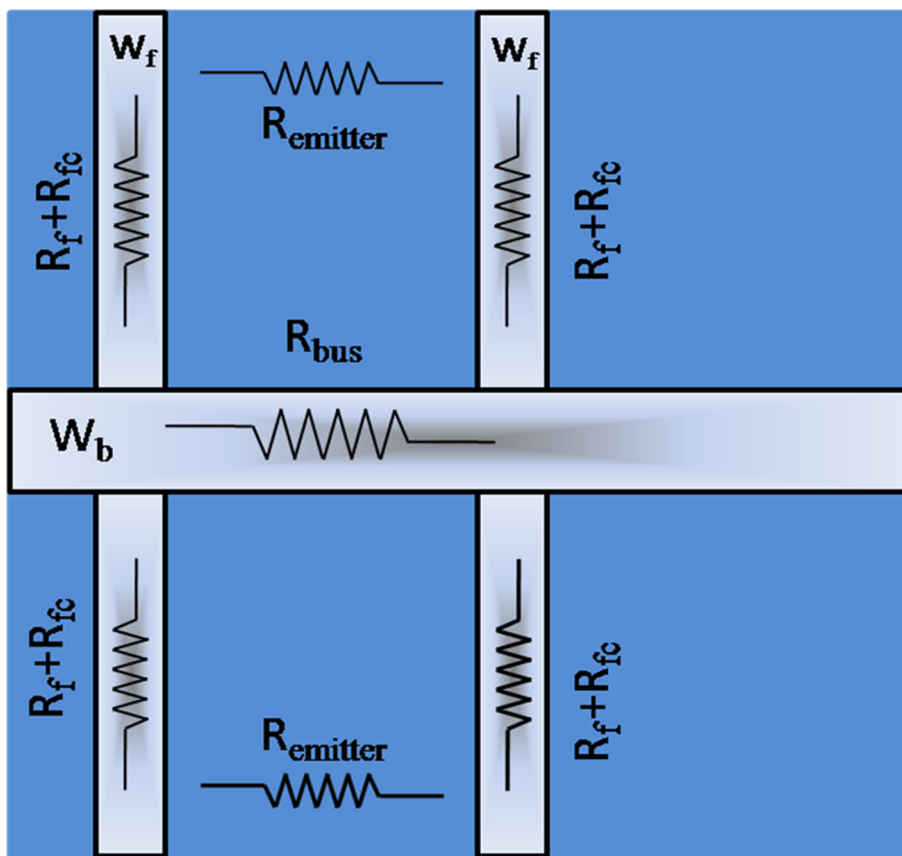


**Fig. 2** Schematic diagram to show the network of the resistive terms of a silicon wafer-based solar cell



and  $R_p$  represent the equivalent resistances forms (see supplementary information for more details).

Further, the recombination losses ( $R_{LOSS}$ ), thermalization losses ( $Th_{LOSS}$ ) and spatial relaxation losses ( $S_{LOSS}$ ) have been calculated using the theory outlined by Ding et al. [48]:

$$R_{LOSS} = \frac{(J_{SC} - J_m)(E_g + k_B T)}{q} \tag{5}$$

$$Th_{LOSS} = \frac{J_{SC} \{ \overline{h\nu} - [E_g + k_B T] \}}{q} \tag{6}$$

$$S_{LOSS} = \frac{J_m (E_g + k_B T - qV_m)}{q} \tag{7}$$

where  $J_{SC}$  represents the short-circuit current density,  $J_m$  and  $V_m$  represent the current density and voltage at the maximum power point, respectively,  $E_g$  represents the bandgap of the Si, and  $\overline{h\nu}$  represents the average photon energy absorbed by Si semiconductor estimated to be 1.32 eV under AM1.5G spectrum for the crystalline silicon [49].

The performance parameters of the silicon solar cell, namely,  $J_{SC}$ , open-circuit voltage ( $V_{OC}$ ) and the fill factor (FF), represent the extent of pseudo-rectangular shape for the nonlinear  $J-V$  curve and the efficiency ( $\eta$ ) of solar cell given by following expression:

$$\eta = \frac{P_{MAX}}{(A \times P_{in})} \tag{8}$$

Here,  $P_{in}$  represents the power input through the incident light radiation. The maximum power output of a solar cell ( $P_{MAX}$ ) can be expressed in terms of performance parameters as given below:

$$P_{MAX} = FF \times V_{OC} \times J_{SC} \tag{9}$$

### 3 Experimental details

The experimental study has been performed with  $J-V$  measurements of the solar cells under full illumination (FI) and with area variation under PS. Commercially available multicrystalline silicon wafer-based solar cells with aluminum back surface field (Al-BSF) in laminated form have been purchased from module manufacturer (Topsun Energy Ltd., Gandhinagar), and the solar cells follow standard  $n^+ - p - p^+$  structure. The testing has been performed using solar simulator (SS80AAA, Photoemission Tech., USA) and source measurement unit (U2722A, Agilent). The solar cells have been tested under standard test condition (AM1.5G,  $1000 \text{ W m}^{-2}$ ) for FI and PS conditions as described in Fig. 3. The active area of the solar cell has been fixed as  $2.5 \times 2.5 \text{ cm}^2$

**Fig. 3** Silicon solar cell schematic under AM1.5G,  $1000 \text{ W m}^{-2}$  radiation. **a** full illumination (FI) and **b** partial shading (84%PS) conditions

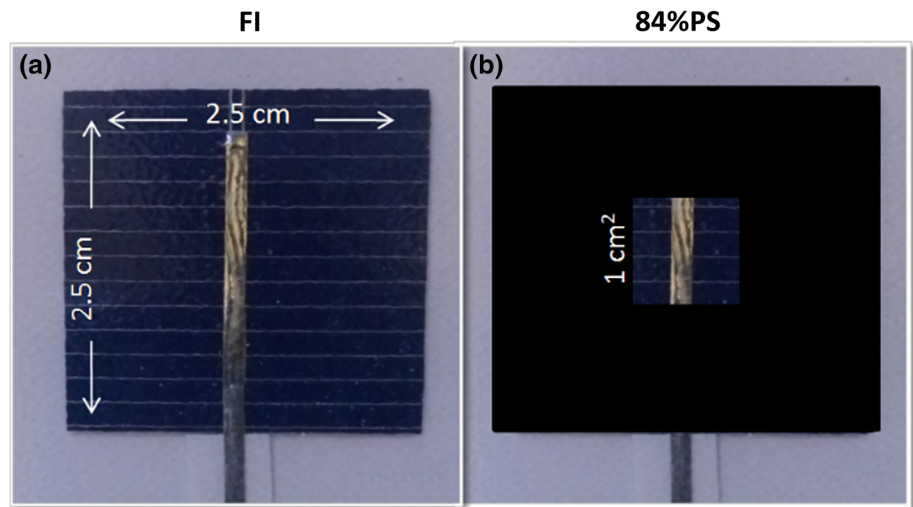


**Table 1** Fitting and output parameters of  $J$ - $V$  characteristics using two-diode model

Parameters	Exp. $J_{SC}$ ( $\text{mA cm}^{-2}$ )	$J_{SC}$ ( $\text{mA cm}^{-2}$ )	Exp. $V_{OC}$ (V)	$V_{OC}$ (V)	$n$	$m$	$R_S$ ( $\Omega$ )	$R_{Sh}$ ( $\Omega$ )	$\eta$ (%)
FI	37.84	37.79	0.62	0.615	1.3	2.5	0.2	5000	18.31
25%PS	19.20	19.19	0.60	0.595	1.7	2.8	0.21	4000	8.44
50%PS	13.30	13.29	0.59	0.590	1.7	2.8	0.23	3900	5.79
60%PS	10.10	10.09	0.59	0.585	1.7	2.8	0.24	3700	4.28
84%PS	5.45	5.00	0.55	0.550	1.7	2.8	0.24	3750	2.01

under FI, and the numbers with percentage sign (25, 50, 60 and 84%) indicate the percentage of shading on solar cells under PS. The cells were shaded in a square shape by using black opaque tape. Further, the effect of other shape of shading has also been studied and included in the Supplementary Information file. All the  $J$ - $V$  measurements have been normalized with respect to area of  $1 \text{ cm}^2$  for the comparison and analysis purpose.

## 4 Results and discussions

### 4.1 Impact of PS on $J$ - $V$ characteristics

The  $J$ - $V$  performance of silicon solar cells subjected to PS with respect to different percentage of shading area (%PS) has been measured under standard test condition. The experimental results have been fitted with the two-diode model to evaluate the performance parameters. The fitting parameters and performance output are listed in Table 1.

Figure 4 depicts the measured and simulated  $J$ - $V$  characteristics for various %PS. It has been observed that the pseudo-rectangular shape significantly deviates from initial behavior due to the influence of PS. The  $J_{SC}$  decreases gradually from 37.84 to 19.20, 13.3, 10.10 and 5.45  $\text{mA cm}^{-2}$  with the increase in shading area of 25, 50, 60 and 84%PS, respec-

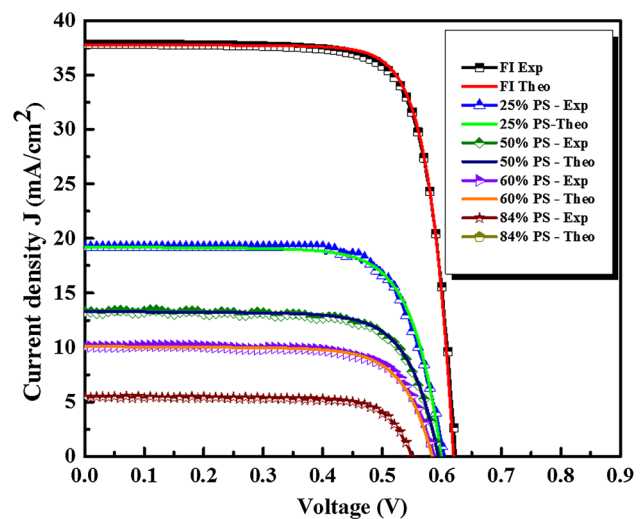


**Fig. 4** Measured and two-diode fitted  $J$ - $V$  characteristics for various PS conditions

tively. The decreasing trend in  $J_{SC}$  signifies a lower generation of charge carriers and inefficient collection through the emitter material under PS. In addition, the  $V_{OC}$  also decreases significantly from 0.62 to 0.59 V due to PS. The reduction in  $V_{OC}$  is attributed to the downward movement of quasi-Fermi level of electrons and the diffusive transport of charge carriers from illuminated region to shaded region due to concentra-

tion gradient. The shift in quasi-Fermi levels due to the local variation of electron concentration in the conduction band in PS regions can be explained by the following equations:

$$E_{Fn} - E_{Fi} = k_B T \ln \left( \frac{n}{n_i} \right) \tag{10}$$

$$E_{Fp} - E_{Fi} = -k_B T \ln \left( \frac{p}{n_i} \right) \tag{11}$$

$$V_{OC} = E_{Fn} - E_{Fp} \tag{12}$$

Under FI condition, the upward shift in electron quasi-Fermi level ( $E_{Fn}$ ) with respect to the intrinsic energy level ( $E_{Fi}$ ) is calculated to be 0.42 eV using the Eq. (10), whereas the upward shift under PS condition remains only 0.12 eV. Here, the number of electron–hole pairs generated under FI is assumed to be  $10^{17}$  and  $10^{15} \text{ cm}^{-3}$  under PS [50]. Using Eq. (11), the downward shift in hole quasi-Fermi level ( $E_{Fp}$ ) with respect to the ( $E_{Fi}$ ) is calculated as 0.42 eV for FI conditions, whereas the shift under PS condition remains 0.12 eV. This calculation shows the decrease in the gap between quasi-Fermi levels of the electrons and the holes under PS as compared to FI, which leads to a lower  $V_{OC}$ . It is observed that the efficiency ( $\eta$ ) of Si solar cell decreases from 18.31 to 2% as shading area increases up to 84%PS. The decrease in  $\eta$  can be correlated with the increase in  $R_S$  and decrease in  $R_{Sh}$  from 0.2 to 0.24  $\Omega$  and 5000 to 3000  $\Omega$ , respectively, using two-diode model. Moreover, the junction quality has been determined by the ideality factors  $n$  and  $m$ , which signifies the recombination in QNR and SCR, respectively. It is observed that the  $n$  and  $m$  increases from 1.3 to 1.7 and from 2.3 to 2.8, respectively, under PS which is mainly due to enhanced recombination. The increase in  $n$  and  $m$  indicates the increase in recombination of charge carriers due to lateral flow of charge carriers in the emitter region and subse-

quent recombination through the intermediate energy levels offered by the shadowed region of the solar cell under PS.

### 4.2 Energy loss analysis under PS

The  $J$ – $V$  characteristic performances under FI and PS are further analyzed by energy balance terminology to account various associated losses as described by Eqs. (5)–(7). The reduction in  $J$ – $V$  characteristics under various %PS has been regulated by the recombination losses, thermalization losses and spatial relaxation losses. Figure 5a, b shows the loss analysis considering above mentioned factors for FI and 50%PS, respectively. It is observed that the recombination loss increases for 50%PS, which is mainly dependent on the difference between  $J_{SC}$  and  $J_m$  according to Eq. (5). In contrast, a marginal change is observed in thermalization loss ( $Th_{LOSS}$ ) under PS as compared to FI condition by using Eq. (6). It is to be noted that the temperature has been kept constant ( $T = 300 \text{ K}$ ) for all the energy loss calculations. Furthermore, the spatial relaxation loss ( $S_{LOSS}$ ) calculated by using Eq. (7) does not show a major impact on the reduction in  $J$ – $V$  as compared to recombination losses. The visual representation of the energy losses as a function of position ( $x$ ) of charge carriers in terms of spatial relaxation, thermalization and trapping under PS is shown in Fig. 6. The increase in the recombination can be correlated to the lateral movement of charge carriers in emitter region due to concentration gradient created by PS. As it is seen from Fig. 6a, d, the spatial relaxation energy gradually decreases under PS, which signifies that the potential energy of charge carriers decreases while relocating from FI to PS region with respect to position. This gradual decrement in the potential energy of the charge carriers leads to recombination of charge carriers (Fig. 6a). Figure 6b schematically represents the energy loss of the charge carriers with decreasing mobility with respect to the

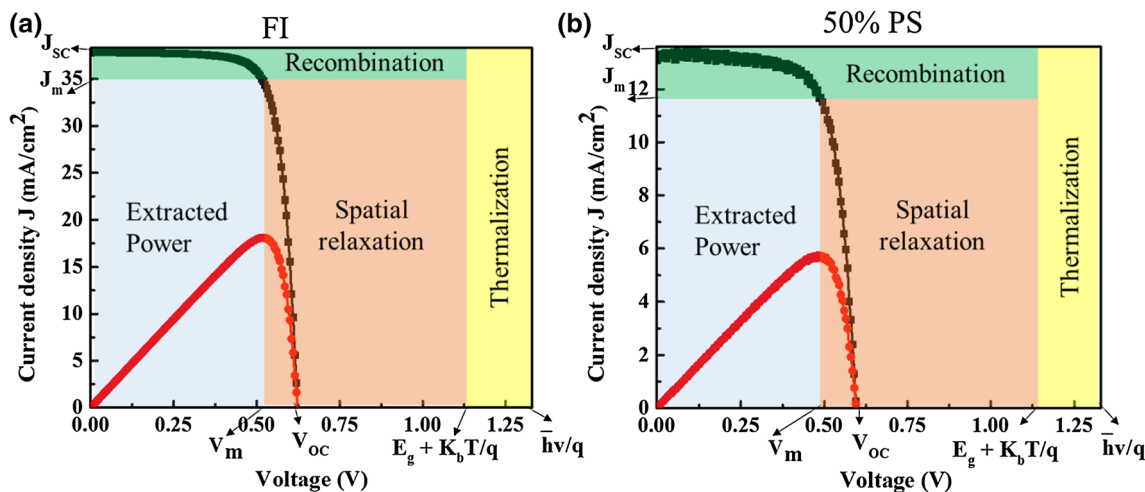
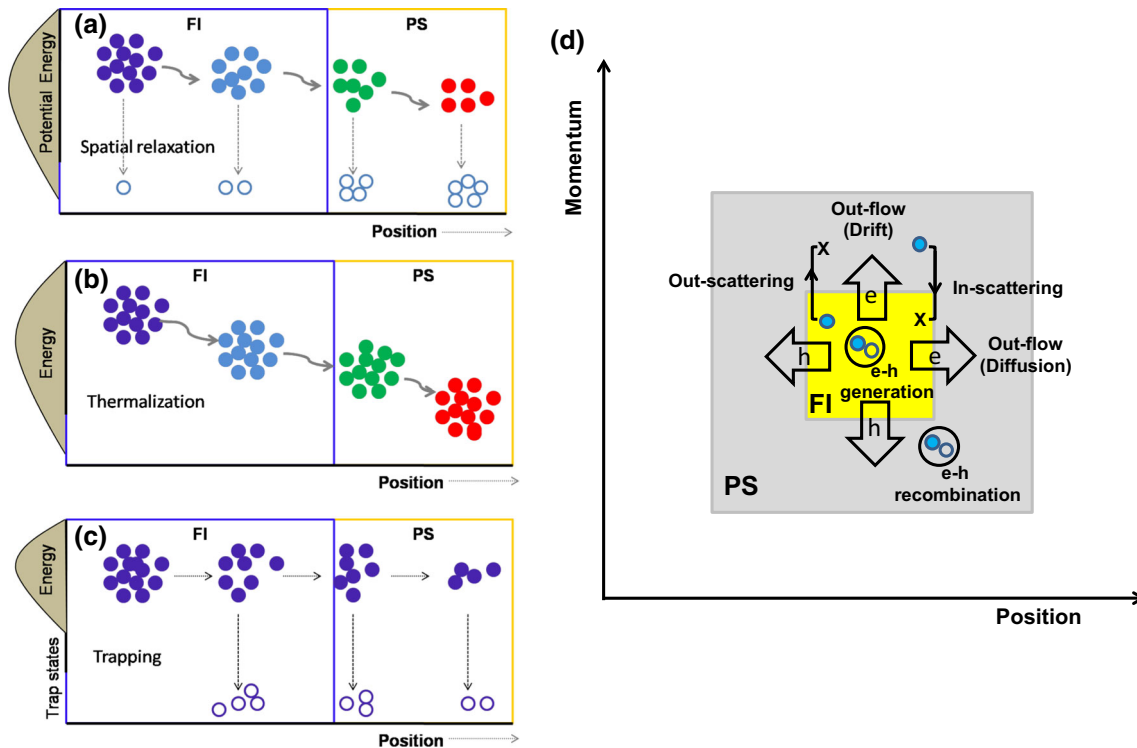


Fig. 5 Energy loss analysis for a FI and b 50%PS conditions



**Fig. 6** Visual representation of the energy losses as function of position ( $x$ ) of charge carriers in terms of **a** spatial relaxation, **b** thermalization and **c** trapping under PS condition. **d** Si solar cell with FI and PS regions

position ( $x$ ), when it undergoes from FI to PS. The energy of the charge carriers decreases with the persistent reduction in mobility, so-called thermalization loss concerning with movements of carriers over FI to PS. Figure 6c visualizes the trapping effect, one of the probable reasons accounts for the recombination of the charge carriers under PS. The trap states offer the recombination platform during the movement of charge carriers from FI to PS region. The availability of trap states increases due to the mismatch of the quasi-Fermi levels of FI and PS region of the solar cell creating a virtual interface for the recombination of the mobile charge carriers. The number of charge carriers decreases due to the recombination while moving from FI to PS, which leads toward lower  $J_{SC}$  under PS. Figure 6d demonstrates the possibility of the reduction in  $J_{SC}$  and  $V_{OC}$ , in terms of the spatial movement of charge carriers under PS. The quasi-Fermi level depends on the electron distribution function ( $f$ ) and also the motion of electrons in the coordinate space. Moreover, the change in the momentum is influenced by the force field acting on the electrons under PS. The electrons may also get transferred into or out of the FI region by collisions/scattering interactions with the secondary electrons. According to Eq. (13), the total rate of change in electron distribution function ( $f$ ), can be written as [51],

$$\begin{aligned} \frac{df}{dt} &= -v \cdot \nabla_r f - F \cdot \nabla_p f + \frac{\partial f}{\partial t} + s(r, p, t) \\ \Rightarrow \frac{df}{dt} + v \cdot \nabla_r f + F \cdot \nabla_p f &= \frac{\partial f}{\partial t} + s(r, p, t) \end{aligned} \quad (13)$$

This change in the distribution function  $\left(\frac{\partial f}{\partial t}\right)$  can be explained into different possible phenomena as follows: (1)  $\left(\frac{\partial f}{\partial t}\right)_{\text{force}} = -\mathbf{F} \cdot \nabla_p f$ , represents the change in the distribution function due to local forces. Where  $\mathbf{F} = \frac{d\mathbf{p}}{dt} = \hbar \frac{d\mathbf{k}}{dt} = q(\mathbf{E} + \mathbf{v} \times \mathbf{B})$ , the total force is equal to the sum of the force due to the locally generated electric field (due to the p–n junction as well as difference in the carrier density) and the Lorentz force due to the magnetic flux density,  $\mathbf{B}$  (as a result of the motion of electrons with the device), (2) the term  $\left(\frac{\partial f}{\partial t}\right)_{\text{diff}} = -\mathbf{v} \cdot \nabla_r f$ , represents the spatial variation in the electron distribution function due to concentration or temperature gradients, both of which result in a diffusion of carriers from the FI region to the PS region of the solar cell under illumination, (3)  $\left(\frac{\partial f}{\partial t}\right)_{\text{coll}}$  is the collision term representing rate of change of the distribution function due to collisions, or scattering which equals the difference between the in-scattering and the out-scattering processes, (4)  $s(r, p, t)$  represents generation–recombination processes

which play significant role on the electrical performance of the device. Out of the above listed processes, the possibility of the spatial variation in the electron distribution  $\left(\frac{\partial f}{\partial t}\right)_{diff}$  and the recombination,  $s(r, p, t)$  processes are most dominating factors responsible for decreasing the charge carrier concentration under the PS condition. Therefore, among all the losses the major reduction in  $J-V$  performance is due to the recombination and spatial relaxation losses under PS. Moreover, the decrease in the carrier concentration reduces the  $V_{OC}$  and thus, the overall  $\eta$  of the Si solar cells.

### 4.3 Effect of surface recombination losses on EQE under PS

To elucidate the recombination within solar cells subjected to PS, the external quantum efficiency (EQE) has been analyzed to understand the reduction in  $J_{SC}$ . The shape of EQE is influenced by front and back surface recombination losses, optical losses and bulk recombination. In order to correlate recombination losses with various %PS, the EQE curves have been determined for FI and various %PS by employing PC1D simulation. The PC1D simulation software has been widely used to simulate various electrical and optical characteristics performance of silicon solar cells [52,53]. The PC1D simulations have been carried out by fitting the experimental  $J-V$  curves for FI and various %PS using bulk lifetime ( $\tau_{n/p}$ , n or p in suffix represent electron or hole, respectively) and surface recombination velocity ( $S_{n/p}$  for front surface and

$S_{nb/pb}$  for back surface) as variable input parameters. The input parameters are listed in Table 2, and output parameters are listed in Table 3 (includes variable input parameters). The EQE curves show gradual decrement as shading percentage increases as shown in Fig. 7. The blue response of EQE (300–450 nm) shows significant reduction from 30 to 0.7% with respect to increase in %PS. The lower blue response signifies that with increase in %PS the front surface recombination velocity increases from 100 to  $10^5$  cm/s as listed in Table 3. Further, the decrease in EQE also indicates low absorption of photons in shorter wavelength under PS. Furthermore, the reduction in EQE in the wavelength range from 450 to 900 nm reflects the high bulk recombination due to the low carrier life time of generated charge carriers with increase in %PS. In the wavelength range of 900–1150 nm, the EQE decreases significantly due to low absorption of longer wavelengths and low carrier lifetime under PS resulting in the low charge carrier collection. A low charge carrier collection indicates a higher recombination at back surface under PS. High surface recombination at the front and back surface results in a significant reduction in  $J_{SC}$  from 37.84 to 5.48 mA cm<sup>-2</sup>.

**Table 2** List of input parameters used for PC1D simulation

Sl. No.	Parameter	Value
1	Area (cm <sup>2</sup> )	6.25 (initial)
2	Thickness (μm)	180
3	Bandgap ( $E_g$ ) at 300 K (eV)	1.12
4	Intrinsic concentration $n_i$ (cm <sup>-3</sup> )	$1 \times 10^{10}$
5	Base doping p-type (cm <sup>-3</sup> )	$1.5 \times 10^{16}$
6	Emitter doping n-type (cm <sup>-3</sup> )	$2.7 \times 10^{20}$

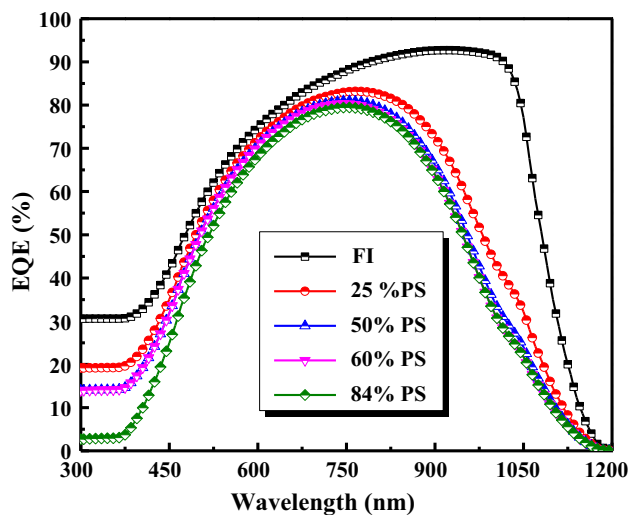


**Fig. 7** External quantum efficiency (EQE) of c-Si solar cells simulated by PC1D for FI and different %PS

**Table 3** Output and variable input parameters for EQE calculation in PC1D simulation

PS (%)	Exp. $J_{SC}$ (mA cm <sup>-2</sup> )	PC1D $J_{SC}$ (mA cm <sup>-2</sup> )	Exp. $V_{OC}$ (V)	PC1D $V_{OC}$ (V)	Bulk recombination		Front surface recombination		Back surface Recombination	
					$\tau_n$ (μs)	$\tau_p$ (μs)	$S_n$ (cm s <sup>-1</sup> )	$S_p$ (cm s <sup>-1</sup> )	$S_{nb}$ (cm s <sup>-1</sup> )	$S_{pb}$ (cm s <sup>-1</sup> )
FI	37.84	32.58	0.62	0.64	100	100	100	50	150	120
25%PS	19.2	20.00	0.60	0.59	2	30	$10^4$	$5 \times 10^4$	$5 \times 10^4$	$10^4$
50%PS	13.3	12.36	0.59	0.58	1	10	$5 \times 10^4$	$10^5$	$10^5$	$5 \times 10^4$
60%PS	10.10	10.03	0.59	0.58	0.8	5	$10^5$	$10^5$	$10^5$	$10^5$
84%PS	5.45	3.84	0.55	0.56	0.5	5	$10^5$	$10^5$	$10^5$	$10^5$

Furthermore, to envisage the effect of front surface recombination on overall power loss, Griddler simulation has been performed for various %PS. The Griddler simulation software is integrated with two-dimensional FEM model supported with MATLAB programme [54,55]. The Griddler simulation software consists of a meshing algorithm and steady-state solver with the arbitrary front metallization geometries to simulate  $J$ - $V$  characteristics of a solar cell [54]. The main input parameters for the Griddler simulation included as wafer type, cell length, metallization pattern, short-circuit current density ( $J_{SC}$ ), number of busbars ( $N_b$ ), number of front fingers ( $N_f$ ), busbar width ( $W_{busbar}$ ), finger sheet resistance, finger contact resistance, layer sheet resistance. The input parameters values of  $N_b$ ,  $W_{busbar}$ , finger sheet resistance and finger contact resistance have been taken as 1, 14, 70  $\mu\text{m}$ ,  $3 \times 10^{-4}$   $\text{m}\Omega/\text{sq.}$  and  $0.35$   $\text{m}\Omega\text{ cm}^2$ , respectively (Table 4). The  $J$ - $V$  performance and corresponding losses have been obtained for FI and various %PS, by varying  $J_{SC}$  value of solar cell area not covered by the front grid. The  $J_{SC}$  value of  $40.2$   $\text{mA cm}^{-2}$  has been assumed for FI [56]. The Griddler simulation has been carried out by varying  $J_{SC}$  in the range of  $40$ – $6$   $\text{mA cm}^{-2}$  for FI to 84%PS in order to fit the experimental data. Figure 8 depicts the pie chart of power losses encountered due to front surface recombination loss,

**Table 4** List of input parameters for Griddler simulation

Parameters	Values
Wafer type	Square
Cell length (cm)	2.5
Metallization pattern	Full area metal contact
Number of busbar	1
Width of busbar (cm)	0.2
Number of front fingers	14
Width of finger ( $\mu\text{m}$ )	70
Finger sheet resistance ( $\text{m}\Omega/\text{sq.}$ )	$3.00 \times 10^{-4}$
Finger contact resistance ( $\text{m}\Omega\text{ cm}^2$ )	0.35

front resistive and shading loss with respect to power output for FI and 84%PS. It is clearly seen that the most dominant power loss mechanism is the front surface recombination, which is found to be 6.73 and 76.54% for FI and 84%PS, respectively. This can be well corroborated by the decrease in the blue response of EQE (see Fig. 7) due to the high surface recombination velocity of charge carriers under shading effect. Figure 9a–d depicts the statistical variation of electrical performance parameters extracted from two-diode model, PC1D and Griddler simulation software with respect to FI and %PS. The  $J_{SC}$  and  $\eta$  decrease drastically with respect to increase in %PS as compared to  $V_{OC}$  and FF. The  $J_{SC}$  and  $V_{OC}$  depend on the amount of extracted electron–hole pairs which decreases with the increase in recombination under increasing %PS.

#### 4.4 Resistance analysis

The resistive losses play an important role in the reduction of  $J$ - $V$  performance under PS. There are various reports on the effect of front and rear side resistive losses on electrical performance. In the present work, we have calculated the resistance and the power losses by doing resistance analysis using Eq. (S1)–(S8) (see supplementary information). The effect of emitter and bulk resistance on the power losses have been studied for FI and PS. It is to be noted that the active area of the solar cell for FI and 50%PS has been taken into consideration as the one of the variable parameters for the calculation. The active area of Si solar cell for FI and 50%PS conditions has been calculated by subtracting the area of the front metal contact grid which comes out to be 5.50 and 2.64  $\text{cm}^2$ , respectively.

The value of emitter resistance ( $R_e$ ) changes from 0.16  $\Omega$  to 0.71  $\Omega$  for FI and 50%PS, respectively, as listed in Table 5. Similarly, the value of bulk resistance ( $R_{bulk}$ ) changes from 0.0012 to 14.3  $\text{m}\Omega$  for FI and 50%PS, respectively. The change in the value of  $R_e$  and  $R_{bulk}$  mainly affects the series resistance, which changes from 0.19  $\Omega$  to 0.23  $\Omega$  as calcu-

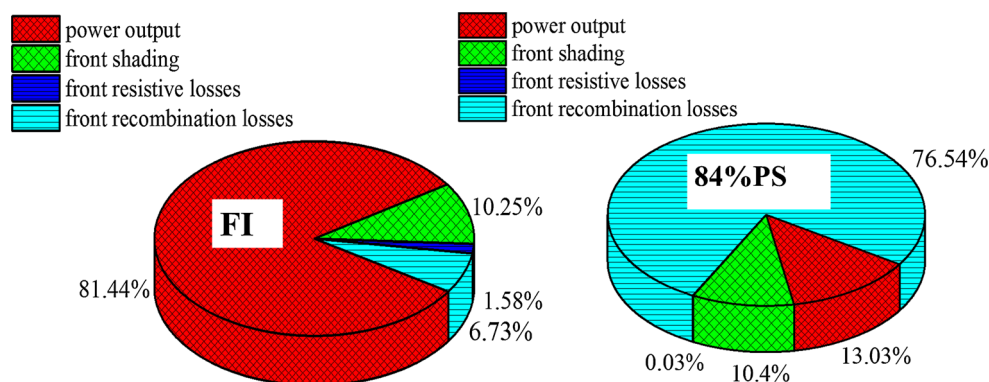


**Fig. 8** Effect of the front surface recombination on the power output loss simulated by Griddler under FI and 84%PS



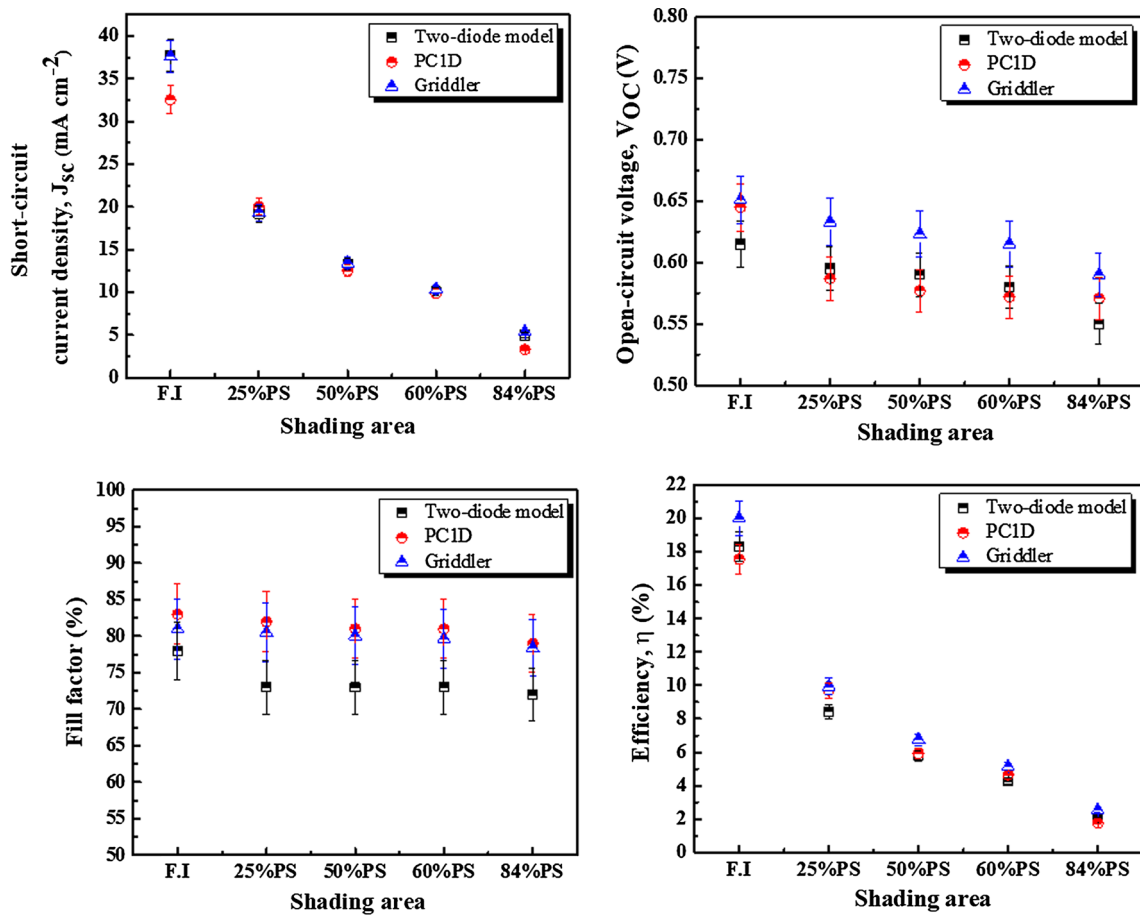


**Fig. 9** Statistical variation in electrical performance parameters  $J_{sc}$ ,  $V_{OC}$ , FF,  $\eta$  simulated by two-diode model, PC1D and Griddler as function of shading area

**Table 5** Series resistance calculation using resistance analysis under FI and PS condition

Sr. No	Parameters	FI	50%PS
1	$R_{bus}$ (m $\Omega$ )	3.11	3.11
2	$R_{fc}$ (m $\Omega$ )	5.71	8.1
3	$R_f$ ( $\Omega$ )	0.357	0.25
4	$R_c$ (m $\Omega$ )	0.166	0.71
5	$R_{bulk}$ ( $\mu\Omega$ )	0.0012	14.3
6	$R_{pp+}$ ( $\Omega$ )	0.01	0.01
7	$R_{Al}$ ( $\Omega$ )	0.01	0.01
8	$N$	14	10
9	$R_s$ ( $\Omega$ )	0.19	0.23

lated using Eq. (4) for FI and 50%PS, respectively, and is in agreement with the two-diode model predictions (Table 1). Furthermore, the calculated emitter power loss ( $P_e$ ) using Eq. (S9) is found to be 34% for 50%PS as compared to the initial power. The  $P_e$  has been attributed to the loss of charge carriers due to recombination at front side governed by PS.

## 5 Conclusions

The reduction in the  $J-V$  performance due to various recombination losses has been critically addressed for c-Si solar cells subjected to various %PS. The experimental  $J-V$  characteristics for various %PS have been analyzed by fitting two-diode model. The change in diode ideality factors and reduction in  $J_{sc}$  are mainly influenced by the recombination of generated charge carriers laterally moving toward the shaded region due to concentration gradient. The realignment of quasi-Fermi levels under PS results in the decrease in  $V_{OC}$  from 0.62 to 0.55 V. The reduction in EQE has been simulated by PC1D and explained in terms of the front surface and bulk recombination as the most dominant factors responsible for the reduction in overall efficiency from 18.31 to 2%. The front surface recombination has been quantified by using Griddler simulation software, which is found to be 6.73 and 76.54% for FI and 84%PS, respectively. The power loss of 34% encountered for the emitter region confirms higher front surface recombination under PS. This study provides a better insight into the recombina-

tion losses associated to partial shading and its consequences for the reduction in the overall efficiency of silicon solar cell.

## 6 Supplementary information

The supplementary information consists of the calculation details of the series resistance. Figure S1 demonstrates the effect of the change shape of shading on the  $J$ - $V$  characteristics of the solar cell.

**Acknowledgements** The authors acknowledge Dr. Pankaj Yadav for the technical help and would like to thank the Solar Research and Development Center (SRDC), PDPU for providing the facilities and their support.

## References

- Jamil, W.J., Abdul Rahman, H., Shaari, S., Salam, Z.: Performance degradation of photovoltaic power system: Review on mitigation methods. *Renew. Sustain. Energy Rev.* **67**, 876–891 (2017)
- Maghami, M.R., Hizam, H., Gomes, C., Radzi, M.A., Rezadad, M.I., Hajighorbani, S.: Power loss due to soiling on solar panel: A review. *Renew. Sustain. Energy Rev.* **59**, 1307–1316 (2016)
- Mani, M., Pillai, R.: Impact of dust on solar photovoltaic (PV) performance: research status, challenges and recommendations. *Renew. Sustain. Energy Rev.* **14**, 3124–3131 (2010)
- Tripathi, B., Yadav, P., Rathod, S., Kumar, M.: Performance analysis and comparison of two silicon material based photovoltaic technologies under actual climatic conditions in Western India. *Energy Convers. Manag.* **80**, 97–102 (2014)
- Sarver, T., Al-Qaraghuli, A., Kazmerski, L.L.: A comprehensive review of the impact of dust on the use of solar energy: history, investigations, results, literature, and mitigation approaches. *Renew. Sustain. Energy Rev.* **22**, 698–733 (2013)
- Ramli, M.A.M., Prasetyono, E., Wicaksana, R.W., Windarko, N.A., Sedraoui, K., Al-Turki, Y.A.: On the investigation of photovoltaic output power reduction due to dust accumulation and weather conditions. *Renew. Energy* **99**, 836–844 (2016)
- Lopez-Garcia, J., Pozza, A., Sample, T.: Long-term soiling of silicon PV modules in a moderate subtropical climate. *Sol. Energy* **130**, 174–183 (2016)
- Mejia, F., Kleissl, J., Bosch, J.L.: The effect of dust on solar photovoltaic systems. *Energy Procedia* **49**, 2370–2376 (2013)
- Mekhilef, S., Saidur, R., Kamalisarvestani, M.: Effect of dust, humidity and air velocity on efficiency of photovoltaic cells. *Renew. Sustain. Energy Rev.* **16**, 2920–2925 (2012)
- Bhol, R., Dash, R., Pradhan, A., Ali, S.M.: Environmental effect assessment on performance of solar PV panel. In: IEEE International Conference Circuit, Power and Computing Technologies, ICCPCT (2015)
- Pavan, A.M., Tassarolo, A., Barbini, N., Mellit, A., Lughì, V.: The effect of manufacturing mismatch on energy production for large-scale photovoltaic plants. *Sol. Energy* **117**, 282–289 (2015)
- Ibrahim, A.: Effect of shadow and dust on the performance of silicon solar cell. *J. Basic Appl. Sci. Res.* **1**, 222–230 (2011)
- Elminir, H.K., Ghitas, A.E., Hamid, R.H., El-Hussainy, F., Beheary, M.M., Abdel-Moneim, K.M.: Effect of dust on the transparent cover of solar collectors. *Energy Convers. Manag.* **47**, 3192–3203 (2006)
- Ghazi, S., Sayigh, A., Ip, K.: Dust effect on flat surfaces: a review paper. *Renew. Sustain. Energy Rev.* **33**, 742–751 (2014)
- El-Nashar, A.M.: Seasonal effect of dust deposition on a field of evacuated tube collectors on the performance of a solar desalination plant. *Desalination* **238**, 66–81 (2009)
- Karatepe, E., Boztepe, M., Çolak, M.: Development of a suitable model for characterizing photovoltaic arrays with shaded solar cells. *Sol. Energy* **81**, 977–992 (2007)
- Ju, F., Fu, X.: Research on impact of dust on solar photovoltaic (PV) performance. In: Proceedings International Conference Electronics Control Engineering (ICECE) (2011)
- Arbuzov, Y.D., Evdokimov, V.M., Majorov, V.A., Saginov, L.D., Shepvalova, O.V.: Silicon PV cell design and solar intensity radiation optimization for CPV systems. *Energy Procedia* **74**, 1543–1550 (2015)
- Ryan, P., Vignola, F., McDaniels, D. K.: Solar cell arrays: degradation due to dirt. In: Proceedings of the American Section of the International Solar Energy Society (1989)
- Hajighorbani, S., Radzi, M.A.M., Ab Kadir, M.Z.A., Shafie, S., Khanaki, R., Maghami, M.R.: Evaluation of fuzzy logic subsets effects on maximum power point tracking for photovoltaic system. *Int. J. Photoenergy* **2014**, 719126 (2014)
- Wenham, S.R., Green, M.A., Watt, M.E., Corkish, R., Sproul, A.: *Applied Photovoltaics*, 3rd edn. Routledge, Oxon (2011)
- Ghitas, A.E., Sabry, M.: A study of the effect of shadowing location and area on the Si solar cell electrical parameters. *Vacuum* **81**(4), 475–478 (2006)
- Salvadores, C., Francisco, J.: Shadowing effect on the performance in solar PV-cells. Master's Thesis, University of Gavle (2015)
- Rachchh, R., Kumar, M., Tripathi, B.: Solar photovoltaic system design optimization by shading analysis to maximize energy generation from limited urban area. *Energy Convers. Manag.* **115**, 244–252 (2016)
- Yadav, P., Kumar, A., Gupta, A., Pachauri, R.K., Chauhan, Y.K., Yadav, V.K.: Investigations on the effects of partial shading and dust accumulation on PV module performance. In: Proceedings of International Conference on Intelligent Communication, Control and Devices (2016)
- Vijayalekshmy, S., Bindu, G.R., Iyer, S.R.: A novel zig-zag scheme for power enhancement of partially shaded solar arrays. *Sol. Energy* **135**, 92–102 (2016)
- Liu, L., Meng, X., Liu, C.: A review of maximum power point tracking methods of PV power system at uniform and partial shading. *Renew. Sustain. Energy Rev.* **53**, 1500–1507 (2016)
- Quaschingt, V., Hanitsch, R.: Numerical simulation of current-voltage characteristics of photovoltaic system with shaded solar cells. *Sol. Energy* **56**, 513–520 (1996)
- Ji, Y.H., Jung, D.Y., Kim, J.G., Kim, J.H., Lee, T.W., Won, C.Y.: A real maximum power point tracking method for mismatching compensation in PV array under partially shaded conditions. *IEEE Trans. Power Electron.* **26**, 1001–1009 (2011)
- Alajmi, B.N., Ahmed, K.H., Finney, S.J., Williams, B.W.: A maximum power point tracking technique for partially shaded photovoltaic systems in microgrids. *IEEE Trans. Power Electron.* **60**, 1596–1606 (2013)
- Guo, S., Walsh, T., Aberle, A., Peters, M.: Analysing partial shading of PV modules by circuit modelling. In: 38th IEEE Photovoltaic Specialists Conference (2012)
- Gao, L., Dougal, R.A., Liu, S., Iotova, A.P.: Parallel-connected solar PV system to address partial and rapidly fluctuating shadow conditions. *IEEE Trans. Power Electron.* **56**, 1548–1556 (2009)
- Feldman, J., Singer, S., Braunstein, A.: Solar cell interconnections and the shadow problem. *Sol. Energy* **26**, 419–428 (1981)
- Lu, F., Guo, S., Walsh, T.M., Aberle, A.G.: Improved PV module performance under partial shading conditions. *Energy Procedia* **33**, 248–255 (2013)

35. Silvestre, S., Chouder, A.: Effects of shadowing on photovoltaic module performance. *Prog. Photovolt. Res. Appl.* **16**, 141–149 (2008)
36. Sera, D., Baghzouz, Y.: On the impact of partial shading on PV output power. In: 2nd International Conference on Renewable Energy Sources (RES'08) (2008)
37. Luo, H., Wen, H., Li, X., Jiang, L., Hu, Y.: Synchronous buck converter based low-cost and high-efficiency sub-module DMPPT PV system under partial shading conditions. *Energy Convers. Manag.* **126**, 473–487 (2016)
38. Sabry, M., Ghitas, A.E.: Effect of edge shading on the performance of silicon solar cell. *Vacuum* **80**, 444–450 (2006)
39. Stutenbaeumer, U., Mesfin, B.: Equivalent model of monocrystalline, polycrystalline and amorphous silicon solar cells. *Renew. Energy* **18**, 501–512 (1999)
40. Gignlach, W., Schlangenotto, H., Maeder, H.: On the radiative recombination rate in silicon. *Phys. Stat. Sol.* **13**, 277–283 (1972)
41. Saha, S.K., Farhan, A.M., Reba, S.I., Ferdous, S.I., Chowdhury, Md.I.B.: An analytical model of dark saturation current of silicon solar cell considering both SRH and auger recombination. In: Proceedings of Regional Symposium on Micro and Nanoelectronics (RSM2011) (2011)
42. Huang, X., Fu, H., Chen, H., Lu, Z., Ding, D., Zhao, Y.: Analysis of loss mechanisms in InGaN solar cells using a semi-analytical model. *J. Appl. Phys.* **119**, 213101–213108 (2016)
43. Belghachi, A.: Detailed analysis of surface recombination in crystalline silicon solar cells. In: International Renewable and Sustainable Energy Conference (IRSEC) (2013)
44. Nelson, J.: *The Physics of Solar Cells*. Imperial College London, London (2003)
45. Solanki, C.S.: *Solar Photovoltaics Fundamentals, Technologies and Application*. PHI Learning Private Limited, New Delhi (2009)
46. Handy, R.J.: Theoretical analysis of the series resistance. *Solid-State Electron.* **10**, 765–775 (1967)
47. Chaudhari, V.A., Solanki, C.S.: From 1 Sun to 10 Suns c-Si cells by optimizing metal grid, metal resistance, and junction depth. *Int. J. Photoenergy* **2009**, 827402 (2009)
48. Ding, D., Johnson, S.R., Yu, S.-Q., Wu, S.-N., Zhang, Y.-H.: A semi-analytical model for semiconductor solar cells. *J. Appl. Phys.* **110**, 123104–123121 (2011)
49. Würfel, P.: *Physics of Solar Cell*. Wiley-VCH Verlag GmbH & Co., New York (2005)
50. Sero, I.M., Belmonte, G.G., Boix, P.P., Vazquez, M.A., Bisquert, J.: Impedance spectroscopy characterisation of highly efficient silicon solar cells under different light illumination intensities. *Energy Environ. Sci.* **2**, 678–686 (2009)
51. Vasilevska, D., Goodnick, S.M.: *Computational Electronics*. Morgan & Claypool Publishers, San Rafael (2006)
52. Fellmeth, T., Mack, S., Bartsch, J., Erath, D., Jäger, U., Preu, R., Clement, F., Biro, D.: 20.1% efficient silicon solar cell with aluminum back surface field. *IEEE Electron Device Lett.* **32**(8), 1101–1103 (2011)
53. Michl, B., Rüdiger, M., Giesecke, J., Hermle, M., Warta, W., Schubert, M.: Efficiency limiting bulk recombination in multicrystalline silicon solar cells. *Sol. Energy Mater. Sol. Cells* **98**, 441–447 (2012)
54. Wong, J., Shanmugam, V., Cunnusamy, J., Zahn, M., Zhou, A., Yang, R., Chen, X., Aberle, A., Mueller, T.: Influence of non-uniform fine lines in silicon solar cell front metal grid design. *Prog. Photovoltaics Res. Appl.* **23**(12), 1877–1883 (2015)
55. Wong, J.: Griddler: intelligent computer aided design of complex solar cell metallization patterns. In: IEEE 39th Photovoltaic Specialists Conference (PVSC) (2013)
56. Shanmugam, V., Wong, J., Peters, I., Cunnusamy, J., Zahn, M., Zhou, A., Yang, R., Chen, X., Aberle, A., Mueller, T.: Analysis of fine-line screen and stencil-printed metal contacts for silicon wafer solar cells. *IEEE J. Photovolt.* **5**(2), 525–533 (2015)